

Variational Quantum Anomaly Detection: Unsupervised mapping of phase diagrams on a physical quantum computer

Korbinian Kottmann,^{1,*} Friederike Metz,^{2,*} Joana Fraxanet,¹ and Niccolo Baldelli¹

¹*ICFO - Institut de Ciències Fotoniques, The Barcelona Institute of Science and Technology,
Av. Carl Friedrich Gauss 3, 08860 Castelldefels (Barcelona), Spain*

²*Quantum Systems Unit, Okinawa Institute of Science and Technology Graduate University,
1919-1 Tancha, Onna, Okinawa 904-0495, Japan*

(Dated: May 16, 2022)

One of the most promising applications of quantum computing is simulating quantum many-body systems. However, there is still a need for methods to efficiently investigate these systems in a native way, capturing their full complexity. Here, we propose variational quantum anomaly detection, an unsupervised quantum machine learning algorithm to analyze quantum data from quantum simulation. The algorithm is used to extract the phase diagram of a system with no prior physical knowledge and can be performed end-to-end on the same quantum device that the system is simulated on. We showcase its capabilities by mapping out the phase diagram of the one-dimensional extended Bose Hubbard model with dimerized hoppings, which exhibits a symmetry protected topological phase. Further, we show that it can be used with readily accessible devices nowadays and perform the algorithm on a real quantum computer.

I. INTRODUCTION

Since the discovery of Shor’s algorithm [1], there have been many attempts to leverage the power of quantum computers to outperform classical computers [2]. One of the most promising near- and far-term applications is simulating quantum many-body systems. With recent experimental advancements [3, 4], there is hope that quantum fault-tolerance can be reached [5], which would enable universal quantum simulation algorithms like phase estimation [2, 6], or adiabatic quantum computation [7]. Currently, we only have access to noisy intermediate-scale quantum (NISQ) devices [8]. There are several proposals for algorithms on these devices like the variational quantum eigensolver (VQE) [9], the quantum approximate optimization algorithm (QAOA) [10], or the quantum autoencoder [11, 12], that employ parameterized circuits which are optimized through a classical feedback loop, typically with gradient based methods [13–15]. These approaches can suffer from so-called Barren plateaus, the phenomenon of an exponentially vanishing gradient of the loss function [16]. In practice, this issue only occurs for large systems and can be avoided by using shallow circuits and local cost functions [17].

With the rise of deep learning in the 2010s, the term *quantum machine learning* was coined in 2016 [18], referring to leveraging quantum computers for linear algebra tasks such as matrix inversion in sub-polynomial time via the Harrow-Hassidim-Lloyd algorithm [19]. One famous use-case was the quantum recommendation system algorithm with an exponential quantum speed-up at the time [20], which inspired classical analogs of the algorithm

with the same, sub-polynomial, complexity (termed as *quantum-inspired* machine learning algorithms) [21]. Today, quantum machine learning refers to using quantum circuits as neural networks [22], or kernel functions [23] to perform classical machine learning tasks like supervised learning [24, 25]. There are cases, where quantum models have provable advantages over classical models [26], but it has been argued that these instances are special cases and no quantum speed up is to be expected for quantum machine learning with classical data [27].

On the other hand, applying classical machine learning to quantum physics has been a great success story [28], most prominently for the classification and mapping of phase diagrams [29–31]. These methods rely on classical data and are therefore restricted by the available classical simulation methods. With physical devices surpassing system sizes that are classically tractable [32], there is need for methods to investigate physical quantum states with quantum computers.

In this paper, we propose a quantum machine learning algorithm for *quantum data*. The data are ground states of quantum many-body systems that are prepared by a quantum simulation subroutine and serve as the input for *Variational Quantum Anomaly Detection* (VQAD). Our quantum anomaly detection scheme belongs to the category of variational quantum algorithms where the circuit *learns* characteristic features of the input state [33]. This can in principle be leveraged for obtaining physical insights of the system from training [34] and is in contrast to previous proposals that are based on kernel methods (one-class support vector machines) [35, 36]. Specifically, we use it to map out an unknown phase diagram of a system without requiring knowledge about the order parameter or the number and location of the different phases.

In anomaly detection, the task is to differentiate *normal* data from *anomalous* data, which is in contrast to supervised learning tasks, where a fixed set of classes with

* These two authors contributed equally
Korbinian.Kottmann@icfo.eu
Friederike.Metz@oist.jp

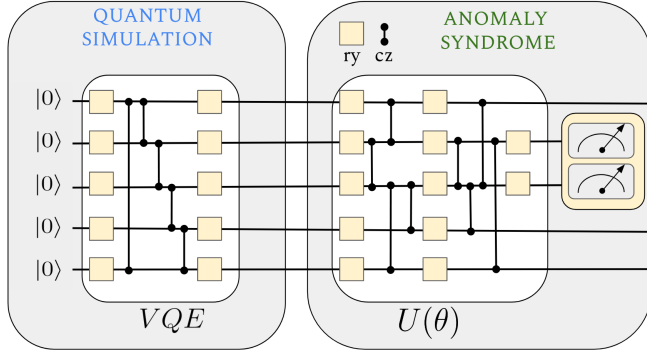


FIG. 1: Overview of our proposal. First, the quantum states are prepared via VQE. Then, they are processed through the anomaly syndrome, consisting of a parameterized unitary $U(\theta)$ and a measurement of a subset of qubits, referred to as trash qubits. ry indicates a parameterized y-axis rotation and cz a (fixed) controlled-z gate.

labels for training are differentiated. On the other hand, the task of anomaly detection requires an *anomaly syndrome*, i.e., an observable that is trained to be of a certain value (typically 0) when *normal* data is input, and be significantly larger for *anomalous* data it is tested on. In classical machine learning, anomaly detection has already been used to extract phase diagrams in an unsupervised fashion from simulated and experimental data [37–39]. VQAD allows us to perform anomaly detection directly *on* a quantum computer, and, with programmable devices readily available, we demonstrate it experimentally on a real device.

II. PROPOSAL

The task of detecting anomalies in ground states of quantum-many body Hamiltonians can be loosely divided into two sub tasks: Preparing the ground state for specific Hamiltonian parameters, and computing an anomaly syndrome indicating whether the state corresponds to a *normal* example or an anomaly. An overview of our proposed algorithm is shown in Fig. 1. For the problem of ground state preparation we define a parameterized circuit ansatz and optimize it using the Variational Quantum Eigensolver (VQE) [9, 40]. The VQE algorithm iteratively minimizes the expectation value of a Hamiltonian with the ansatz circuit to find the ground state by optimizing the parameters of the circuit via a quantum-classical feedback loop. In this work we employed the VQE implementation provided by the Qiskit library [41] and optimized it using simultaneous perturbation stochastic approximation (SPSA) [42, 43].

Once the ground state is prepared on the quantum device a subsequent circuit serves as the anomaly syndrome. Our circuit ansatz is inspired by the recently proposed quantum auto-encoder, which similar to its classi-

cal counterpart can be used for compression of classical and quantum data [11, 12]. It is composed of several layers each consisting of parameterized single qubit y-rotations and controlled-z gates. After the final layer a predefined number n_t of *trash* qubits is measured in the computational basis. The objective is to decouple the trash qubits from the rest of the system, effectively compressing the original ground state into a fewer number of qubits. The circuit parameters are then optimized to faithfully compress states that are considered *normal*. However, when the optimized circuit is tested on anomalous states not seen during training, it is expected that the circuit fails to decouple the trash qubits from the rest of the system. To quantify the degree of decoupling we use the Hamming distance d_H of the trash qubit measurement outcomes to the $|0\rangle^{\otimes n_t}$ state, i.e., the number of 1s in a bit-string of measurement outcomes. The cost function C can then be defined as the Hamming distance averaged over several circuit evaluations $C = 1/N \sum_i^N d_{Hi}$, where N is the number of performed measurements or shots. The cost function can also be rewritten in terms of expectation values of local Pauli-z operators Z_j

$$C = \frac{1}{N} \sum_{i=1}^N d_{Hi} = \frac{1}{2} \sum_{j=1}^{n_t} (1 - \langle Z_j \rangle). \quad (1)$$

The VQAD circuit achieves perfect compression if the trash qubits are fully disentangled from the remaining qubits and mapped into the pure $|0\rangle^{\otimes n_t}$ state resulting in a cost equal to zero.

The specific circuit ansatz for the anomaly syndrome is shown in Fig. 1 for the case of $n_t = 2$ trash qubits. Each layer of the circuit starts with parameterized single-qubit y-rotations applied to every qubit followed by a sequence of entangling controlled-z gates. The currently available NISQ devices are inherently noisy and the computations are subject to gate errors. To minimize the number of two-qubit gates we apply the controlled-z gates only between trash qubits and non-trash-qubits instead of an all-to-all entangling map [12]. In a single layer each non-trash qubit will be coupled to exactly one trash qubit. This entangling scheme is repeated in the subsequent layers until every non-trash qubit has been coupled to each trash qubit exactly once. After the final layer additional single-qubit y-rotations act on the trash qubits before they are being measured.

Note that in principle the trash qubits can be placed anywhere in the circuit, however, when performing computations on a real quantum device it proved advantageous to explicitly take the qubit connectivity structure of the device into account in order to reduce the number of required SWAP operations. Our experiments are performed on IBMQ quantum devices with a linear connectivity and hence we placed the trash qubits in the middle of the device architecture.

In our proposed circuit ansatz the number of circuit layers depends linearly on the number of trash qubits and does not scale with the total number of qubits as long as

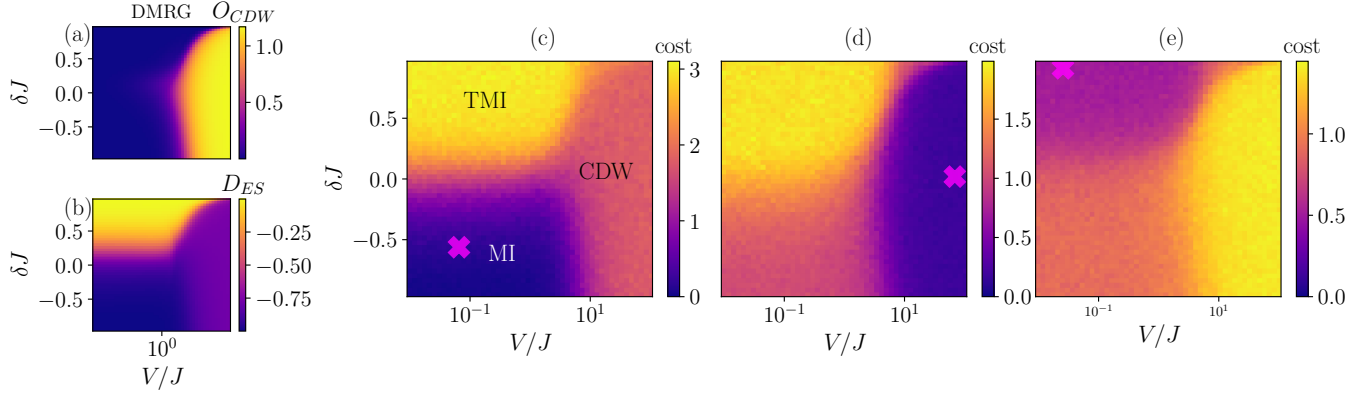


FIG. 2: (a)-(b) Phase diagram of the DEBHM from Eq. (2) using (a) the order parameter corresponding to the CDW, O_{CDW} , and (b) the degeneracy of the entanglement spectrum, D_{ES} . The results were obtained from DMRG for a system of length $L = 12$ at half filling $\bar{n} = 0.5$. We fix the maximum bond dimension $BD = 50$ and the maximum number of bosons per site to $n_0 = 1$. (c)-(e) Cost/anomaly syndrome of a VQAD trained on a single ground state (indicated by a cross) of the $L = 12$ DEBHM in the (c) MI phase using 6 trash qubits, the (d) CDW phase using 4 trash qubits, and the (e) TMI phase using 2 trash qubits. The cost at each data point is the Hamming distance averaged over 1000 measurement shots using an ideal quantum device simulator.

the number of trash qubits is kept fixed. Therefore, the circuit is of constant (shallow) depth and together with the fact that the cost function is composed of only local operators, the training is expected to not suffer from Barren plateaus [17]. We train the circuit representing the anomaly syndrome on *normal* data points only using SPSA and subsequently test it on a data set containing both *normal* and anomalous data points. The latter can be inferred through an increase in the cost function signaling that the corresponding ground state cannot be fully compressed by the optimized circuit. We stress again that our method belongs therefore to the category of unsupervised learning tasks since it does not require labeled training data and thus no prior knowledge about the quantum system apart from the Hamiltonian.

III. RESULTS

A. Simulations with ideal quantum data

In order to test the performance of VQAD, we first study the one-dimensional extended Bose Hubbard model with dimerized hoppings (DEBHM) [44], which is described by the following Hamiltonian

$$H = - \sum_{i=1}^{L-1} (J + \delta J (-1)^i) (b_i^\dagger b_{i+1} + \text{h.c.}) + \frac{U}{2} \sum_i n_i (n_i - 1) + V \sum_i n_i n_{i+1}, \quad (2)$$

where $b_i^\dagger (b_i)$ is the bosonic operator representing the creation(annihilation) of a particle at site i of a lattice of length L . The tunneling amplitudes $J - \delta J$ ($J + \delta J$)

indicate hopping processes on odd (even) links connecting two nearest-neighbor sites, while V represents the nearest-neighbor (NN) repulsion. Here, we take the hardcore boson limit, i.e., the on-site repulsion $U/J \rightarrow \infty$, such that the local Hilbert space is two-dimensional and each site can only accommodate 0 or 1 bosons. This model can be effectively mapped into a spin-1/2 system [45].

Previous studies of the DEBHM model at half filling ($\bar{n} = 0.5$) have demonstrated the existence of three distinct phases [44]. For small and intermediate values of V/J and $\delta J > 0$, we find a topological Mott insulator (TMI) displaying features analogous to a symmetry protected topological phase appearing in the dimerized spin-1/2 bond-alternating Heisenberg model [45]. On the other hand, for negative values of δJ we expect a trivial Mott insulator (MI), while in the regime where the nearest-neighbor repulsion dominates, a charge density wave (CDW) appears.

In Fig. 2(a-b), we study the phase diagram of the model in Eq. (2) in terms of its parameters δJ and V using the density matrix renormalization group algorithm (DMRG) [46–48]. In order to differentiate between the Mott insulating and the CDW phases one can compute the order parameter

$$O_{CDW} = \sum_{i=1}^{L/2} (-1)^i \delta n_i \quad (3)$$

which is shown in Fig. 2(a) [49]. To characterize the TMI we study the entanglement spectrum (ES) which is expected to be doubly degenerate in a topologically non-trivial phase [50] due to the existence of edge states. The entanglement spectrum $\{\lambda_i\}$ is defined in terms of the positive real-valued Schmidt coefficients $\{\alpha_i\}$ of a

bipartite decomposition of the system by $\alpha_i^2 = \exp(-\lambda_i)$. In Fig. 2(b), we plot the degeneracy of the ES,

$$D_{ES} = \sum_i (-1)^i e^{-\lambda_i}. \quad (4)$$

The D_{ES} vanishes only for small NN interaction strengths V and positive values of δJ , while the trivial MI and CDW phases do not show a degeneracy and hence do not host topological edge states.

In the following, we test the capabilities of the VQAD with ideal states obtained from DMRG simulations. The anomaly syndrome is trained using a single representative ground state within one of the phases such that the cost measured at the trash qubits is minimised and the states of this phase can be efficiently compressed by the circuit. Afterwards, the trained circuit processes all states from the full phase diagram, ideally with similarly low cost in the same phase and significantly higher cost in other phases.

In Fig. 2 c)-e) we show the resultant cost landscapes for three circuits each optimized at a different point in the phase diagram. Indeed, ground states outside of the training phase give rise to a large cost and hence are correctly classified by the VQAD as anomalous. Surprisingly, a single ground state example (indicated by the cross) was sufficient to successfully train the VQAD and infer all three phases. Similar results were recently reported for the case of classical anomaly detection using neural network auto-encoders [39].

To demonstrate the robustness of the VQAD against noise present in currently available NISQ devices we apply a depolarizing noise channel after each gate with error probabilities $p_{\text{err}} = 0.001$ (single-qubit gates) and $p_{\text{err}} = 0.01, 0.07$ (two-qubit gates) and show two exemplary cost profiles of the trained anomaly detector in Fig. 3. While it is not possible to reach a cost of zero in the training phase, the optimization still converges and all three phases can be successfully inferred.

B. Experiments on a real quantum computer

We have seen that with ideal quantum data, VQAD can map out non-trivial phase diagrams including topologically non-trivial phases with and without noise in the anomaly syndrome. Next, we discuss its performance in real-noise simulations, that is with noise profiles and qubit connectivities from a real quantum device. Furthermore, we perform the quantum simulation subroutine, i.e., the ground state preparation via VQE, on the same circuit. For this task, we consider the paradigmatic transverse longitudinal field Ising (TLFI) model [51]

$$H = J \sum_{i=1}^L Z_i Z_{i+1} - g_x \sum_{i=1}^L X_i - g_z \sum_{i=1}^L Z_i, \quad (5)$$

where X_i, Z_i are the Pauli matrices on site i , J is the coupling strength, and g_x, g_z are the transverse and longitudinal fields, respectively. For $g_z = 0$ the model

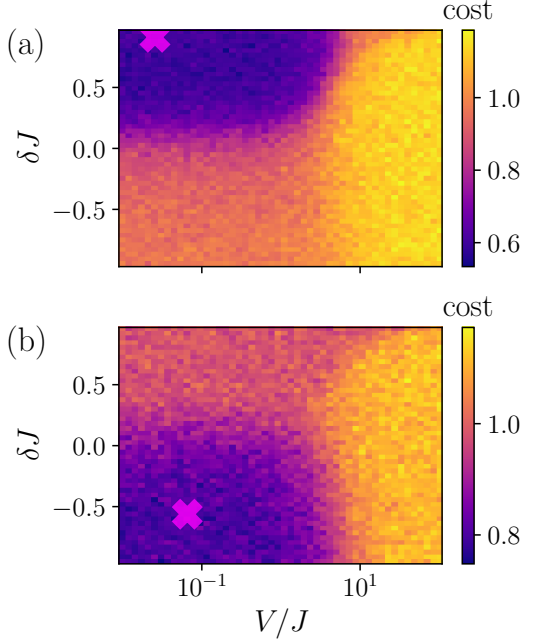


FIG. 3: Cost of a VQAD trained on a single ground state (marked by the cross) of the DEBHM with $L = 12$ sites. The gates of the VQAD circuit are subject to depolarizing noise with $p_{\text{err}} = 0.001$ (single-qubit gates) and (a) $p_{\text{err}} = 0.01$, (b) $p_{\text{err}} = 0.07$ (two-qubit gates). The chosen values are motivated by the error probabilities of real devices.

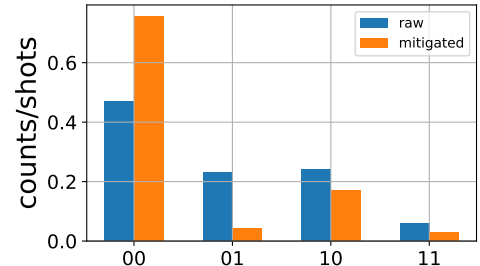


FIG. 4: Comparison of the trash qubit measurement outcomes with and without measurement error mitigation. The anomaly syndrome circuit has been trained with and without error mitigation on a ground state of the TLFI model in the ordered phase in real-noise simulations. Ideally, all of the 1000 shots would result in the 00 bit string. By mitigating the measurement errors we improve the results towards this desired outcome.

is exactly solvable and shows a quantum phase transition from a ferromagnetic (antiferromagnetic) phase for $g_x/J < 1$ and J negative (positive) to a paramagnetic one for $g_x/J > 1$ [52]. In the following we set $J = 1$ and vary the longitudinal and transverse fields. In this regime the model is not exactly solvable and the phase diagram has been extensively studied numerically [53, 54].

The antiferromagnet-paramagnet quantum phase transition is best characterized by the order parameter which in this case is the staggered magnetization

$$\hat{S} = \sum_{i=1^L} (-1)^i \frac{Z_i}{L}. \quad (6)$$

We simulate the ground states of the Hamiltonian in Eq. (5) using VQE for $L = 5$. On a noisy device, long-range entangling gates are performed by consecutive local two-qubit gates (SWAP operation), increasing the actual circuit depth. A large number of consecutive gates leads to decoherence due to gate errors and destroys the results. With the circuit presented in Fig. 1 for the VQE subroutine, we found a trade-off between expressibility and noise tolerance with a cyclic entanglement distribution and only one layer. Additionally, we performed measurement error mitigation [55], which can further improve the results of the cost function as seen in Fig. 4.

For small values of g_x and g_z , in the ferromagnetic ordered phase, the ground states $\psi \simeq |10101\rangle$ ($\langle \hat{S} \rangle = 1$) and $\psi \simeq |01010\rangle$ ($\langle \hat{S} \rangle = -1$) have a similar energy, which is why the optimization can get stuck in local minima. Hence, in the ordered phase, VQE can converge to both a state with positive or negative staggered magnetization, or an equal superposition of the two as can be seen in Fig. 5 a). The VQAD simulation results in Fig. 5 b) show a perfect correlation between positive $\langle S \rangle$ and low cost, and vice versa, negative $\langle S \rangle$ and high cost - which, intuitively, can be expected [56]. The disordered phase is detected from the plateau of high cost (~ 1).

We see that VQAD also performs well under realistic conditions, so we next test the algorithm on a physical device. For this task, we use the $L = 5$ qubits on `ibmq_jakarta` [55]. To avoid jumps in the staggered magnetization in the ordered phase and improve convergence of the VQE optimization, we reuse already optimized parameters at neighboring points in the phase diagram as a good initial guess. Due to a large computation time overhead per execution on the real device, we additionally prepared pre-optimized parameters for both subroutines from a realistic noisy simulation, and use these as initial guesses for the optimization on the device. We found that for computing the staggered magnetization it is actually not necessary to re-run the VQE optimization on the physical device, and we can achieve faithful results by directly using the optimized parameters from the simulation as seen in Fig. 6. The resulting cost values for the optimized circuit, plotted in Fig. 6, clearly distinguish the two phases, with the cost from the experiment showing solely an almost constant offset compared to the noisy simulation.

The code to run these simulations and experiments can be found on GitHub [57].

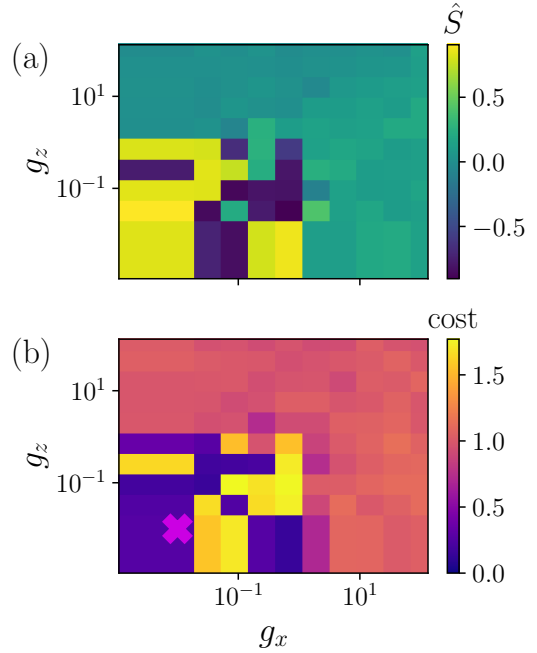


FIG. 5: Real-noise simulations of the staggered magnetization \hat{S} (a) and the anomaly syndrome (b) for the TLF model. We trained the anomaly syndrome in the ordered phase on a state with positive \hat{S} , indicated by the purple cross. Inside the ordered phase, there is a perfect correlation between low cost states for positive \hat{S} , and very high cost where VQE converged to a negative \hat{S} . The paramagnetic phase is detected by a plateau in the anomaly syndrome.

IV. OUTLOOK

We showed that our proposed algorithm is capable of mapping out complex phase diagrams, including topologically non-trivial phases. We further demonstrated that the algorithm also works in realistic scenarios for both real-noise simulations and on a real quantum computer. Hence, we provide a tool to experimentally explore phase diagrams in future quantum devices, which will be especially useful when physical devices surpass the limit of what can be classically computed.

Currently, the main bottleneck of VQAD is the presence of noise in real devices. We were able to improve our anomaly detection scheme by employing measurement error mitigation and adopting the circuits according to the physical device. These results are promising, and with current efforts on enhancing device performances, error mitigation and circuit optimization strategies in the community, we are hopeful to see even further improvements soon.

In this project we focused on using VQAD to extract the phase diagram of a quantum many-body-systems. A possible future extension would be to apply it to the problem of entanglement witnessing and certification in

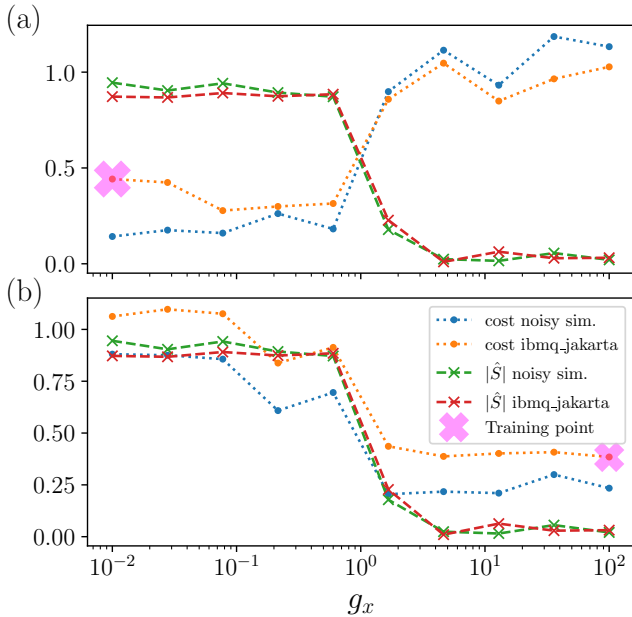


FIG. 6: Real device VQAD experiments: We show the order parameter \hat{S} compared to the VQAD results both for execution on `ibmq_jakarta` and noisy simulators with the same noise profile. We trained on a single ground state in the ordered (a) and paramagnetic (b) phase. For sampling \hat{S} , we use the same parameters for the VQE circuit in simulation and experiment. All values for \hat{S} in the paramagnetic phase are negative, hence, for better visualization we plot its absolute value $|\hat{S}|$. For training the anomaly syndrome, the optimized parameters from the simulation are taken as an initial guess.

many-body scenarios without tomography. Furthermore, the use of an autoencoder-like architecture has the advantage over kernel-based schemes in that there exists tools of interpreting the feature space in classical autoencoders to gain physical insights [34], which can be a possible future extension for the quantum case discussed here.

ACKNOWLEDGMENTS

Acknowledgments The authors thank D. González-Cuadra, L. Barbiero and U. Bhattacharya for discussions on the extended Bose Hubbard model and A. Dauphin and M. Lewenstein for valuable feedback on the manuscript.

This work was supported by the European Union’s Horizon 2020 research and innovation programme under the Marie Skłodowska-Curie grant agreement No 713729 (K.K.). This work was supported by OIST Graduate University and we are grateful for the help and support provided by the Scientific Computing and Data Analysis Section of the Research Support Division at OIST. N.B. acknowledges support from a “la Caixa” Foundation (ID 100010434) fellowship. The fellowship code is LCF/BQ/DI20/11780033. We acknowledge support from ERC AdG’s NOQIA and CERQUTE, Spanish MINECO (FIDEUA PID2019-106901GB-I00/10.13039 / 501100011033, FIS2020-TRANQI, Severo Ochoa CEX2019-000910-S and Retos Quspin), the Generalitat de Catalunya (CERCA Program, SGR 1341, SGR 1381 and QuantumCAT), Fundacio Privada Cellex and Fundacio Mir-Puig, MINECO-EU QUANTERA MAQS (funded by State Research Agency (AEI) PCI2019-111828-2 / 10.13039/501100011033), EU Horizon 2020 FET-OPEN OPTOLogic (Grant No 899794), and the National Science Centre, Poland-Symfonia Grant No. 2016/20/W/ST4/00314.

We acknowledge the use of IBM Quantum services for this work. The views expressed are those of the authors, and do not reflect the official policy or position of IBM or the IBM Quantum team.

Author contributions KK initiated and managed the project, performed the VQAD simulations for the TLFI model, and was in charge of the experiments on the physical device.

FM was in charge of the implementation in Python / Qiskit, worked on the TLFI model and performed the VQAD simulations for the DEBHM.

JF was in charge of DEBHM, the DMRG simulations and performed VQE simulations for the TLFI model.

NB worked on the implementation of the TLFI model and performed VQE simulations, and worked on error mitigation in noisy simulations.

All authors contributed to the discussions and the writing of the manuscript.

[1] P.W. Shor, “Algorithms for quantum computation: discrete logarithms and factoring,” in *Proceedings 35th Annual Symposium on Foundations of Computer Science* (1994) pp. 124–134.
 [2] Michael A. Nielsen and Isaac L. Chuang, *Quantum Computation and Quantum Information: 10th Anniversary Edition* (Cambridge University Press, 2010).
 [3] Giulia Semeghini, Harry Levine, Alexander Keesling,

Sepehr Ebadi, Tout T. Wang, Dolev Bluvstein, Ruben Verresen, Hannes Pichler, Marcin Kalinowski, Rhine Samajdar, Ahmed Omran, Subir Sachdev, Ashvin Vishwanath, Markus Greiner, Vladan Vuletic, and Mikhail D. Lukin, “Probing Topological Spin Liquids on a Programmable Quantum Simulator,” (2021), [arXiv:2104.04119](https://arxiv.org/abs/2104.04119).

[4] K. J. Satzinger, Y. Liu, A. Smith, C. Knapp, M. New-

man, C. Jones, Z. Chen, C. Quintana, X. Mi, A. Dunsworth, C. Gidney, I. Aleiner, F. Arute, K. Arya, J. Atalaya, *et al.*, “Realizing topologically ordered states on a quantum processor,” **(2021)**, arXiv:2104.01180.

[5] Dorit Aharonov and Michael Ben-Or, “Fault-Tolerant Quantum Computation With Constant Error Rate,” *SIAM Journal on Computing* **38**, 1207–1282 (1999), arXiv:9906129 [quant-ph].

[6] A. Yu. Kitaev, “Quantum measurements and the Abelian Stabilizer Problem,” **(1995)**, arXiv:9511026 [quant-ph].

[7] Edward Farhi, Jeffrey Goldstone, Sam Gutmann, and Michael Sipser, “Quantum Computation by Adiabatic Evolution,” **(2000)**, arXiv:0001106 [quant-ph].

[8] John Preskill, “Quantum Computing in the NISQ era and beyond,” *Quantum* **2** (2018), 10.22331/q-2018-08-06-79, arXiv:1801.00862.

[9] Alberto Peruzzo, Jarrod McClean, Peter Shadbolt, Man Hong Yung, Xiao Qi Zhou, Peter J. Love, Alán Aspuru-Guzik, and Jeremy L. O’Brien, “A variational eigenvalue solver on a photonic quantum processor,” *Nature Communications* **5**, 1–7 (2014).

[10] Edward Farhi, Jeffrey Goldstone, and Sam Gutmann, “A Quantum Approximate Optimization Algorithm,” **(2014)**, arXiv:1411.4028.

[11] Jonathan Romero, Jonathan P Olson, and Alan Aspuru-Guzik, “Quantum autoencoders for efficient compression of quantum data,” *Quantum Science and Technology* **2**, 045001 (2017).

[12] Carlos Bravo-Prieto, “Quantum autoencoders with enhanced data encoding,” *Machine Learning: Science and Technology* (2021).

[13] Jarrod R. McClean, Jonathan Romero, Ryan Babbush, and Alán Aspuru-Guzik, “The theory of variational hybrid quantum-classical algorithms,” *New Journal of Physics* **18** (2015), 10.1088/1367-2630/18/2/023023, arXiv:1509.04279.

[14] James Stokes, Josh Izaac, Nathan Killoran, and Giuseppe Carleo, “Quantum Natural Gradient,” *Quantum* **4** (2019), 10.22331/q-2020-05-25-269, arXiv:1909.02108.

[15] M. Cerezo, Andrew Arrasmith, Ryan Babbush, Simon C. Benjamin, Suguru Endo, Keisuke Fujii, Jarrod R. McClean, Kosuke Mitarai, Xiao Yuan, Lukasz Cincio, and Patrick J. Coles, “Variational Quantum Algorithms,” **(2020)**, arXiv:2012.09265.

[16] Jarrod R. McClean, Sergio Boixo, Vadim N. Smelyanskiy, Ryan Babbush, and Hartmut Neven, “Barren plateaus in quantum neural network training landscapes,” *Nature Communications* **9** (2018), 10.1038/s41467-018-07090-4, arXiv:1803.11173.

[17] M. Cerezo, Akira Sone, Tyler Volkoff, Lukasz Cincio, and Patrick J. Coles, “Cost Function Dependent Barren Plateaus in Shallow Parametrized Quantum Circuits,” *Nature Communications* **12** (2020), 10.1038/s41467-021-21728-w, arXiv:2001.00550.

[18] Jacob Biamonte, Peter Wittek, Nicola Pancotti, Patrick Rebentrost, Nathan Wiebe, and Seth Lloyd, “Quantum machine learning,” *Nature* **549**, 195–202 (2017).

[19] Aram W. Harrow, Avinatan Hassidim, and Seth Lloyd, “Quantum algorithm for solving linear systems of equations,” *Physical Review Letters* **103** (2008), 10.1103/PhysRevLett.103.150502, arXiv:0811.3171.

[20] Iordanis Kerenidis and Anupam Prakash, “Quantum Recommendation Systems,” *Leibniz International Proceedings in Informatics, LIPIcs* **67** (2016), arXiv:1603.08675.

[21] Ewin Tang, “A quantum-inspired classical algorithm for recommendation systems,” *Proceedings of the Annual ACM Symposium on Theory of Computing* , 217–228 (2018), arXiv:1807.04271.

[22] Adrián Pérez-Salinas, Alba Cervera-Lierta, Elies Gil-Fuster, and José I. Latorre, “Data re-uploading for a universal quantum classifier,” *Quantum* **4**, 226 (2020), arXiv:1907.02085.

[23] Maria Schuld, “Supervised quantum machine learning models are kernel methods,” **(2021)**, arXiv:2101.11020.

[24] Edward Farhi and Hartmut Neven, “Classification with Quantum Neural Networks on Near Term Processors,” **(2018)**, arXiv:1802.06002.

[25] Patrick Rebentrost, Masoud Mohseni, and Seth Lloyd, “Quantum support vector machine for big data classification,” *Physical Review Letters* **113** (2013), 10.1103/PhysRevLett.113.130503, arXiv:1307.0471.

[26] Yunchao Liu, Srinivasan Arunachalam, and Kristan Temme, “A rigorous and robust quantum speed-up in supervised machine learning,” **(2020)**, arXiv:2010.02174.

[27] Jonas M. Kübler, Simon Buchholz, and Bernhard Schölkopf, “The Inductive Bias of Quantum Kernels,” **(2021)**, arXiv:2106.03747.

[28] Giuseppe Carleo, Ignacio Cirac, Kyle Cranmer, Laurent Daudet, Maria Schuld, Naftali Tishby, Leslie Vogt-Maranto, and Lenka Zdeborová, “Machine learning and the physical sciences,” *Reviews of Modern Physics* **91** (2019), 10.1103/RevModPhys.91.045002, arXiv:1903.10563.

[29] Juan Carrasquilla and Roger G. Melko, “Machine learning phases of matter,” *Nature Physics* **13**, 431–434 (2016), arXiv:1605.01735.

[30] Evert P. L. van Nieuwenburg, Ye-Hua Liu, and Sebastian D. Huber, “Learning phase transitions by confusion,” *Nature Physics* **13**, 435–439 (2016), arXiv:1610.02048.

[31] Patrick Huembeli, Alexandre Dauphin, Peter Wittek, and Christian Gogolin, “Automated discovery of characteristic features of phase transitions in many-body localization,” *Physical Review B* **99** (2018), 10.1103/PhysRevB.99.104106, arXiv:1806.00419.

[32] Frank Arute, Kunal Arya, Ryan Babbush, Dave Bacon, Joseph C. Bardin, Rami Barends, Rupak Biswas, Sergio Boixo, Fernando G.S.L. Brandao, David A. Buell, Brian Burkett, Yu Chen, Zijun Chen, Ben Chiaro, Roberto Collins, *et al.*, “Quantum supremacy using a programmable superconducting processor,” *Nature* **574**, 505–510 (2019).

[33] The term *learning* is commonly used in (quantum) machine learning and data-driven problem solving to refer to data-specific optimization.

[34] Raban Iten, Tony Metger, Henrik Wilming, Lidia del Rio, and Renato Renner, “Discovering physical concepts with neural networks,” *Physical Review Letters* **124** (2018), 10.1103/PhysRevLett.124.010508, arXiv:1807.10300.

[35] Nana Liu and Patrick Rebentrost, “Quantum machine learning for quantum anomaly detection,” *Physical Review A* **97** (2017), 10.1103/PhysRevA.97.042315, arXiv:1710.07405.

[36] Jin-Ming Liang, Shu-Qian Shen, Ming Li, and Lei Li, “Quantum Anomaly Detection with Density Estimation and Multivariate Gaussian Distribution,” *Phys-*

ical Review A **99** (2019), 10.1103/PhysRevA.99.052310, arXiv:1906.06479.

[37] Korbinian Kottmann, Patrick Huembeli, Maciej Lewenstein, and Antonio Acín, “Unsupervised Phase Discovery with Deep Anomaly Detection,” *Physical Review Letters* **125** (2020), 10.1103/PhysRevLett.125.170603, arXiv:2003.09905.

[38] Niklas Käming, Anna Dawid, Korbinian Kottmann, Maciej Lewenstein, Klaus Sengstock, Alexandre Dauphin, and Christof Weitenberg, “Unsupervised machine learning of topological phase transitions from experimental data,” *Machine Learning: Science and Technology* (2021), arXiv:2101.05712.

[39] Korbinian Kottmann, Philippe Corboz, Maciej Lewenstein, and Antonio Acín, “Unsupervised mapping of phase diagrams of 2D systems from infinite projected entangled-pair states via deep anomaly detection,” (2021), arXiv:2105.09089.

[40] Jarrod R McClean, Jonathan Romero, Ryan Babbush, and Alán Aspuru-Guzik, “The theory of variational hybrid quantum-classical algorithms,” *New Journal of Physics* **18**, 023023 (2016).

[41] Héctor Abraham, AduOffei, Rochisha Agarwal, Ismail Yunus Akhalwaya, Gadi Aleksandrowicz, Thomas Alexander, Matthew Amy, Eli Arbel, Arijit02, Abraham Asfaw, Artur Avkhadiev, Carlos Azaustre, AzizNgoueya, Abhik Banerjee, Aman Bansal, *et al.*, “Qiskit: An open-source framework for quantum computing,” (2019).

[42] J. Spall, “An overview of the simultaneous perturbation method for efficient optimization,” *Johns Hopkins Apl Technical Digest* **19**, 482–492 (1998).

[43] Abhinav Kandala, Antonio Mezzacapo, Kristan Temme, Maika Takita, Markus Brink, Jerry M. Chow, and Jay M. Gambetta, “Hardware-efficient variational quantum eigensolver for small molecules and quantum magnets,” *Nature* **549**, 242–246 (2017).

[44] Koudai Sugimoto, Satoshi Ejima, Florian Lange, and Holger Fehske, “Quantum phase transitions in the dimerized extended bose-hubbard model,” *Phys. Rev. A* **99**, 012122 (2019).

[45] Hai Tao Wang, Bo Li, and Sam Young Cho, “Topological quantum phase transition in bond-alternating spin- $\frac{1}{2}$ heisenberg chains,” *Phys. Rev. B* **87**, 054402 (2013).

[46] Ulrich Schollwöck, “The density-matrix renormalization group in the age of matrix product states,” *Annals of Physics* **326**, 96–192 (2011).

[47] Steven R. White, “Density matrix formulation for quantum renormalization groups,” *Phys. Rev. Lett.* **69**, 2863–2866 (1992).

[48] Johannes Hauschild and Frank Pollmann, “Efficient numerical simulations with Tensor Networks: Tensor Network Python (TeNPy),” *SciPost Phys. Lect. Notes* **5** (2018), code available from <https://github.com/tenpy/tenpy>, arXiv:1805.00055.

[49] In the definition of O_{CDW} , we consider only half of the sites of the system because the DMRG algorithm outputs a symmetric state, which is a superposition of the two degenerate ground states.

[50] Frank Pollmann, Ari M. Turner, Erez Berg, and Masaki Oshikawa, “Entanglement spectrum of a topological phase in one dimension,” *Phys. Rev. B* **81**, 064439 (2010).

[51] H C Fogedby, “The ising chain in a skew magnetic field,” *Journal of Physics C: Solid State Physics* **11**, 2801–2813 (1978).

[52] Subir Sachdev, “Quantum phase transitions,” in *Handbook of Magnetism and Advanced Magnetic Materials* (American Cancer Society, 2007).

[53] Parongama Sen, “Quantum phase transitions in the ising model in a spatially modulated field,” *Phys. Rev. E* **63**, 016112 (2000).

[54] A. A. Ovchinnikov, D. V. Dmitriev, V. Ya. Krivnov, and V. O. Cherenovskii, “Antiferromagnetic ising chain in a mixed transverse and longitudinal magnetic field,” *Phys. Rev. B* **68**, 214406 (2003).

[55] Sergey Bravyi, Sarah Sheldon, Abhinav Kandala, David C. McKay, and Jay M. Gambetta, “Mitigating measurement errors in multiqubit experiments,” *Physical Review A* **103**, 042605 (2021), arXiv:2006.14044.

[56] In a very hand-wavy way, we can understand this as we train the circuit U to perform $U|1010\rangle = |\Psi\rangle \otimes |00\rangle_{\text{trash}}$ such that $U|0101\rangle = |\Psi\rangle \otimes |11\rangle_{\text{trash}}$ if we input a state with opposite ordering.

[57] Korbinian Kottmann, Friederike Metz, Joana Fraxanet, and Niccolo Baldelli, “Variational quantum anomaly detection code on github <https://github.com/Qottmann/Quantum-anomaly-detection>,” (2021).